AIMS Materials Science, 9(6): 808–834.
DOI: 10.3934/matersci.2022050
Received: 12 May 2022
Revised: 06 September 2022
Accepted: 13 September 2022
Published: 25 October 2022

http://www.aimspress.com/journal/Materials

Research article

Effects of pitch length of perforation on the crease bending characteristics of a polypropylene sheet subjected to indentation of a perforation blade

Shigeru Nagasawa[1,2,*] and Tomoki Hosokawa[1]

[1] Department of Mechanical Engineering, Nagaoka University of Technology, 1603-1 Kamitomioka, Nagaoka, Niigata 940-2188, Japan
[2] Faculty of Engineering, Sanjo City University, 1341 Kamisugoro, Sanjo, Niigata 955-0091, Japan

* **Correspondence**: Email: nagasawa.shigeru@sanjo-u.ac.jp, snaga@mech.nagaokaut.ac.jp.

Abstract: This study reveals the bending formability of a polypropylene (PP) sheet indented by a perforation blade when changing the pitch of the dashed-ruled line and the indentation depth. Creasing is a folding method of a carton sheet in which a score (called as a ruled line) is made at the bent portion. When making a creased line on a resin sheet, the scored sheet thickness decreases by applying half cutting or creasing (pressing) at the bent portion to make it easier to fold. To smoothly process a folding line on the resin sheet, a dashed line using a perforation blade is sometimes considered. The pitch length of the dashed line, and its nicked (uncut) length, affect the crease bending characteristics of the resin sheet scored by the perforation blade. However, only a limited number of studies have analyzed the dashed line bending moment response. In this study, to clarify the bending formability of a 0.5-mm-thick PP sheet indented by a developed perforation blade, first, the influence of the perforation pitch length on the crease bending characteristics of a scored PP sheet was investigated from a 0.5-mm fine pitch up to an 8-mm commercially sold pitch with a cutting-to-pitch length ratio of 50%. Second, the nicked zone depth against the cutting tip was set as 50% of the 0.5-mm thickness of the PP sheet. Furthermore, it was revealed that burrs (wedged bottom) in the cut part of the perforated (dashed) line affected the bending moment resistance in the folding process of the scored PP sheet, when changing the indentation depth of the perforation blade.

Keywords: bending; scoring; perforated line; polypropylene; elastic-limitation; plastic collapse; contact interference

Abbreviations: A: cutting length in one cycle pitch (Figure 1), B: nicked length in one cycle pitch (Figure 1); $C = A + B$: pitch length of perforation blade; x: downward (compressive) displacement of the upper holder with perforation blade; F: compressive force applied to the perforation blade with a length (L_B) = 30 mm; W = 24 mm: width of the PP sheet; $f = F/W$: compressive line force applied to the PP sheet; t: thickness of the PP sheet = 0.5 mm; d_1: indentation depth against the PP sheet at the cutting tip (part A); d_2: indentation depth against the PP sheet at nicked (uncut but scored) zone(part B); d_{2R}: residual (permanent) thickness of the PP sheet at the nicked zone after scoring; $d_{2as}/t = 1 - d_{2R}/t$: normalized residual indentation depth of the scored zone; t_{ip}: elapsed time; θ: folding angle of the fixture at the crease stress tester (CST); M: bending moment resistance per unit width (N·mm/mm) measured by the CST; θ_1: CST fixture angle when the first cycle's bending resistance (first starting angle) increases; θ_2: CST fixture angle when the second cycle's bending resistance (second starting angle) increases; M_{p1}: bending moment resistance at the first inflection point in the first cycle; θ_{p1}: angle at the first inflection point; $C_1 = \partial M / \partial \theta|_{\theta=\theta_1}$: first stiffness (gradient of the bending moment resistance with an angle at $\theta = \theta_1$); $C_2 = \partial M / \partial \theta|_{\theta=\theta_2}$: second stiffness (gradient of the bending moment resistance with an angle at $\theta = \theta_2$)

1. Introduction

Clear cartons are resin packaging containers widely used for packaging cosmetics. Since many resin sheets are transparent, the products can be seen through them, which have a display effect that makes the products more appealing. Transparent resin sheets are used in various applications today. To manufacture packaging containers such as paperboard and/or clear cartons, form-cutting and creasing processes are generally applied to a worksheet in the form-cutting process. Creasing (scoring and folding) is a method in which a score, called a ruled line, is applied to the bent portion, and second the scored part is folded [1–3]. When creasing a resin sheet, its scored thickness is decreased by applying half cutting or pressing at the bent portion to make it easier to fold [4,5].

Concerning the creasing of paperboard, to use a plain-uniform round edge blade is suitable for smoothly folding paperboards [6–8]. However, since a polypropylene (PP) sheet is not delaminated by the scoring of the round edge blade, only the indented depth and its scored shape determine the relative strength of the bending stiffness at the scored position, whereas to precisely control the scored depth is generally difficult or unstable. This difficulty is caused by the mechanical-pressing principle of the flat-bed die-cutter [9,10]. Studies have investigated the usage and fundamental properties [11–13], and a couple of research articles exist on the cutting strength of PP [14,15].

Nagasawa et al. studied the edge profile effects on the crease bending characteristics of a 0.3-mm thick PP sheet scored by a plain-uniform two-line wedge blade (not by a perforation) when varying the scored depth [16]. This report revealed that the residual cutting depth (scored depth) sensitively determines the scored profile and the bending moment resistance of the scored part of the PP sheet.

To smoothly process a folding line on a resin sheet such as PP, an alternative processing method is empirically known, compared to a plain-uniform, two-line wedge blade. Namely, a leading crease using a perforation blade (sewing machine blade) is sometimes considered [17,18]. This method can easily determine the indentation depth from the full stroke cutting and combine the designed uncut length. The pitch length of the dashed line, and its nicked (scored, half-cut zone) length, seem to affect the crease bending characteristics of the resin sheet scored by a perforation blade. However, a lack of studies exists concerning the analysis of the bending moment response of scored dashed lines using the perforation blade. The perforation blade was made from a 42º single wedge of a 0.71-mm thick steel rule, which had a part of cutting line segments and a part of scoring (half-cut) line segments on a creasing line.

To clarify the bending formability of a 0.5-mm thick PP sheet indented by a perforation blade, the bending moment response was investigated with the folding angle of the fixture under a specified rotational velocity when varying the pitch of the dashed line and the residual indentation (scored) depth against the PP sheet. When the ratio of cutting-to-pitch length was 50%, the pitch length of the blade was varied in a certain range, and several kinds of perforated (dashed) lines were processed on the PP sheet. The depth of the nicked (removed) zone against the cutting tip was set as D = 0.25 mm, which was 50% of the 0.5-mm thickness of the PP sheet. The residual indentation depth of the nicked (scored) zone was varied in a certain range, from 25% to 75% of the PP sheet, to reveal the effects of the sheard profiles of the cutting and half-cut (scored) line segments on the crease bending characteristics when varying the residual indentation depth. Using these scored PP sheets, the bending moment resistance was investigated with the folding angle of the fixture from the bending-free state (~0º) up to 90º.

2. Materials and experimental methods

2.1. Mechanical characteristics of PP sheet for scoring

Table 1 shows the in-plane mechanical properties of the 0.5-mm thick PP sheet. The strain rate was set as 0.00417 s^{-1} (a tensile velocity of V_{tns} = 0.33 mm/s against an 80-mm clamped distance), and the shape of the PP sheet was set as the JIS K-7127 type-5 (dumbbell type).

Table 1. In-plane mechanical properties of 0.5-mm thick PP sheet (Strain rate: 0.00417 s^{-1} at room temperature and humidity of 297 K and 50 %RH, respectively).

Young's modulus E/GPa	Yield stress σ_Y/MPa	Tensile strength σ_B/MPa at a logarithmic strain of 0.08	Breaking logarithmic strain ε_B/-
1.25	31.9	42.1	1.79

The preliminary tensile testing results revealed that when the tensile velocity increased from V_{tns} = 0.08 up to 8.3 mm/s, the breaking logarithmic strain was less than 0.1 (tends to be brittle, fragile) at V_{tns} =8.3 mm/s, whereas it exceeded 1.6 (tends to be ductile) for V_{tns} < 2.5 mm/s. Moreover, in the case of a 42º wedge indentation into the thickness direction, when choosing an indentation velocity of V = 0.005 mm/s, the in-plane spreading velocity becomes $2V\sin 21º$ = 0.0036 mm/s. Hence, at V = 0.005 mm/s, the in-plane behavior of the PP sheet seems to be ductile, not fragile.

2.2. Mechanical condition of perforation blades

As the original blade material for scoring the PP sheet, a carbon-tool-steel (JIS-G-4401, SK85), 42º single-wedge blade (a commercial-2-point-Thomson knife) was prepared. The blade had tip and body hardness values of 690 and 465 VHN, respectively. Figure 1 shows the profile of the perforation blade, and some parameters are presented in Table 2**.** The length of the perforation blade was 30 mm. The pitch length C was a sum of the cutting part A and the nicked (half-cut) part B (tie width). The A-to-C ratio (A/C) was kept as 0.5 ($A = B = 0.5C$), and C was varied from 0.5–8 mm. The nicked part was machined using wire cutting (EDM) at a depth of $D = 0.25$ mm. The number $n = 24/C$ was the total number of the one cycle pitch formed on a piece of 24-mm width-PP sheet.

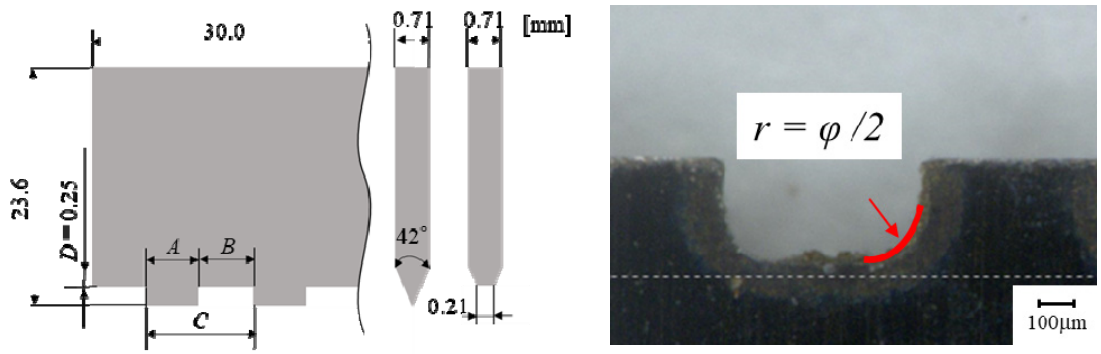

Figure 1. Specification of perforation blade. (a) Definition of perforation blade's dimensions and (b) corner profile in case of 0.5 × 0.5, C = 1 mm (the wire diameter of EDM ϕ = 0.2 mm, r = 0.1 mm).

Table 2. Parameter dimensions of perforation blade based on a 42º single wedge, 0.71-mm (two points)-thick Thomson knife (Figure 1).

Specification	A (mm)	B (mm)	C (mm)	$n = 24/C$	$TPI = 25.4/C$
0.25 × 0.25	0.25	0.25	0.5	48	50.8
0.5 × 0.5	0.5	0.5	1	24	25.4
1 × 1	1	1	2	12	12.7
2 × 2	2	2	4	6	6.35
3 × 3	3	3	6	4	4.23
4 × 4	4	4	8	3	3.18
Plain-uniform	0	30	-	-	-

Figure 2 shows the attitude of the perforation blade against a 24-mm width-PP sheet, and a general view of the prepared perforation blades. For the comparison with the pitch length of the perforation blade, a trapezoidal (plain-uniform) blade with a tip thickness of 0.21 mm (a height of 0.25 mm was uniformly removed, and the estimation was 0.25 × 2tan21º = 0.19 mm) was prepared. According to the online catalog of American Micro Industries Inc. [17], a certain fine pitch dashed line is called "micro perforation" in which the teeth per inch (TPI) is larger than 30 [17,18].

Namely in this study, $C < 0.85$ mm is prepared as a "micro perforation". Due to the restriction of the wire cutting method using a 0.2-mm copper wire, the grooved profile of the nicked (removed) zone had a 0.1-mm radius (Figure 1b). Therefore, the round profile of the grooved corners seemed to affect the three-dimensional deformation of the scored zone (part of B), especially for $C < 1$ mm.

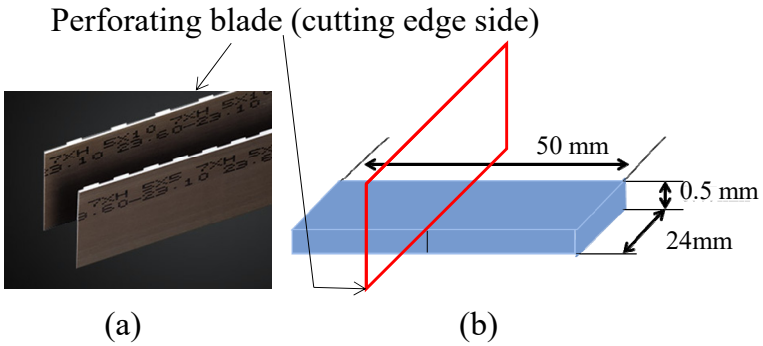

Figure 2. Schematic of perforation blade against PP sheet. (a) General view of blade and (b) attitude of blade against PP sheet.

Since the trapezoidal part of the depth $D = 0.25$ mm was indented to the 0.5-mm thick PP sheet, the cutting and scoring combination was considered as a special specification. Generally, some well-known scoring of perforation is considered as $D > t = 0.5$ mm.

2.3. Compressive loading procedure of blade against sheet

Figure 3 shows schematics of the scoring (pressing) apparatus schematic for making a perforated (dashed) line on a 0.5-mm thick PP sheet with a width and a length of 24 and 50 mm, respectively. The initial step height of a new cutting tip from the rubber fixture was ~3 mm. When pressing the perforation blade against the PP sheet, the cutting part A was indented to the PP sheet until $d_1/t \approx 1$, as well as $d_2/t \approx 0.5$. Generally, since there is an equivalent-spring effect on the blade displacement, the residual (permanent) indentation depth d_{2as} can be estimated principally with the difference between the blade displacement and device elongation. The real (residual) depth d_{2as}/t was ~0.3 when considering $d_1/t \approx 1.0$ under the real indentation of part A. Herein, the device elongation was not calibrated strictly. Alternatively, the residual indentation depth of the perforation blade $d_{2as} = t - d_{2R}$ was calculated from the measured residual thickness d_{2R} after scoring. When inspecting the effect of the pitch C on the crease formability, named Case 1, the residual indentation depth was fixed as $d_{2as}/t = 1 - d_{2R}/t \approx 0.45$ ($d_{2R} = 0.27$–0.28 mm $\approx 0.55t$). There was a little insufficient indentation of blade for scoring the bottom layer of the PP sheet. The applied pushing force F was measured by a load cell.

Before indenting the blade, the PP sheet was gently placed on the counter plate without any fixture. When moving the blade downward, the 7-mm × 7-mm × 50-mm rubber sponge empirically fastened the PP sheet at a 10-mm horizontal distance (Figure 3a). The relationship between the scoring line force F and the displacement of blade holder x against the PP sheet reveals that x increased up $x = d_1$. The surface level of the PP sheet was defined as $x = 0$. The rubber reaction force was calibrated with the scoring force F.

When making the scored PP sheets in Case 1 ($d_{2as}/t = 1 - d_{2R}/t \approx 0.45$), a certain thin uncut layer (Figure 4a) seemed to exist in some samples. or the bottom layer of part *A* seemed to be cut off, but no gap exists (there seemed to be interference of burrs) after scoring (Figure 4b). Therefore, to discuss the effects of the bottom gap at part *A* on the bending moment resistance, another condition of indentation depth (Figure 4c) was considered as Case 2. Herein, the residual indentation depth of the scored PP sheet (at part *B*) was varied in a range of $d_{2as}/t = 1 - d_{2R}/t = 0.25$–$0.75$ when choosing three patterns of perforation: 0.5 × 0.5, 3 × 3 and the plain-uniform trapezoidal.

The indentation velocity of the blade was set as $V = 0.005$ mm/s, and the sample number of PP sheets was mainly $N = 5$ for each perforation blade at room temperature and relative humidity of 296 K and 50%, respectively.

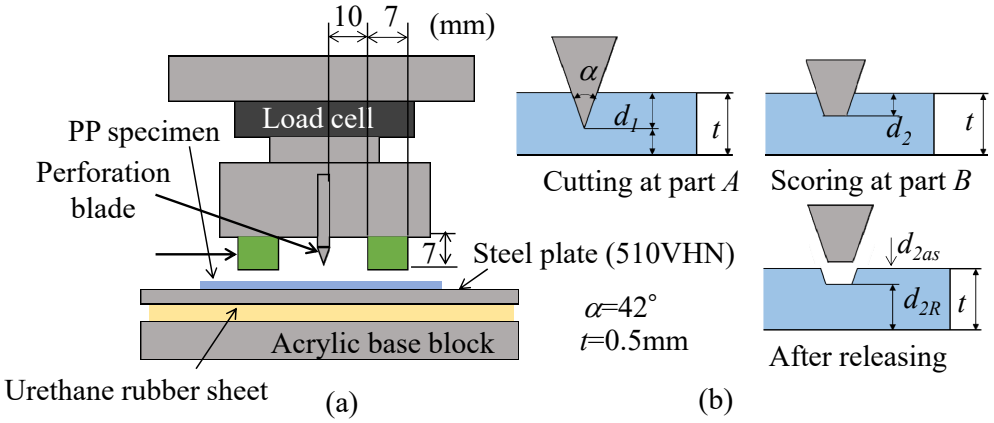

Figure 3. Experimental schematic apparatus for scoring of perforation on PP sheet when choosing $d_1/t \approx 1.1$–1.26 (Case 1). (a) Blade organization: 0.5-mm thick PP sheet, 5-mm thick urethan rubber, 7 mm × 7 mm × 50 mm rubber fixture, and compressive testing machine (10 kN load cell). (b) Scoring state of perforation blade against 0.5-mm thick PP sheet. Here, $d_1 - d_2 = D = 0.25$ mm.

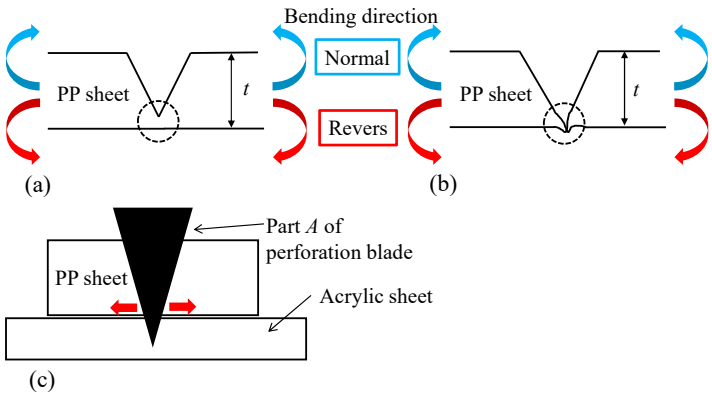

Figure 4. Schematic of state of insufficient cutting off and modification of cutting off under scoring process. (a) Existence of a thin uncut layer, (b) contact interference of burrs (or sheared edges) at the bottom layer, and (c) spread out by over-cutting using a plastic underlay (5-mm-thick acrylic sheet).

2.4. Bending moment response of scored PP sheet

Figure 5 shows a folding (bending) test method using a crease stress tester CST-J1 [19]. The scored side was set up as two patterns: (a) normal folding direction (interior scored notch) and (b) reverse folding direction (exterior scored notch in the folding process from the folding angle θ of θ_1 or θ_2 to 90º). Half of the PP sheet was initially clamped at the scored position by the fixture of the CST-J1, maintaining $\theta = \theta_1$. The origin of the folding angle $\theta = 0$ was defined with the attitude of a flat plate. The rotational velocity of the fixture was $\omega = d\theta/dt_{ep}$ = 0.2 rps (1.257 rad/s), and the arm length ℓ was 10 mm from the scored position to the load cell (rating maximum of 10 N). The bending strain rate $\dot{\varepsilon_b}$ at the scored notch is calculated using Eq 1. Herein, Young's modulus of E = 1.25 GPa (Table 1) and a residual thickness of $d_{2R} = 0.55t$ = 0.275 mm are considered. The rate of bending moment resistance $\dot{M}$ is estimated as a ratio of M_{p1} to θ_{p1}/ω ($M_{p1}\omega/\theta_{p1}$). This value of bending strain rate is calculated later when obtaining the relationship between M_{p1} and θ_{p1}.

$$\dot{\varepsilon_b} = 6\dot{M}/(Ed_{2R}{}^2) = 6M_{p1}\omega/(\theta_{p1}Ed_{2R}{}^2) \quad (1)$$

The first starting angle of θ_1 depends on the warpage of the scored PP sheet. As a tendency of the scored PP sheet when $d_{2as}/t = 1 - d_{2R}/t \approx 0.45$, θ_1 was about −5º in the normal folding, whereas θ_1 was about +5º in the reverse folding. When $0.45 < d_{2as}/t < 0.75$ (a part of Case 2), the amplitude of $|\theta_1|$ increased and $|\theta_1| \approx 15$º at d_{2as}/t = 0.6–0.75.

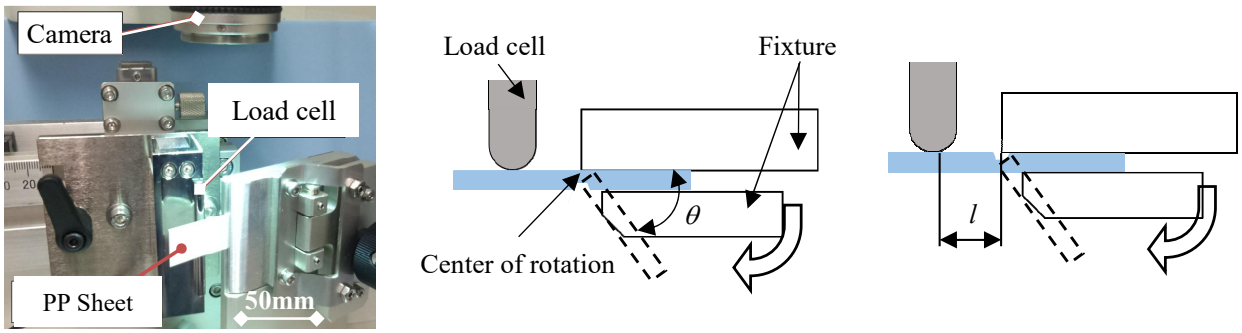

Figure 5. Schematic of folding (bending) test of scored PP sheet. (a) General view of creasing strength tester CST-J1 [19], (b) normal folding direction (inside scored), and (c) reverse folding direction (outside scored).

The folding (bending) test was continuously examined twice until releasing the reaction force of the load cell. For example, in the folding (bending) test of Case 1, when choosing $d_{2as}/t = 1 - d_{2R}/t \approx 0.45$, seven perforations were examined to measure the bending moment resistance M with the folding angle θ in both the normal and reverse folding directions. Figure 6 illustrates a representative example of the M-θ response when choosing the plain-uniform trapezoidal blade (A = 0, B = 30 mm). To detect some features of the M-θ response, when varying the pitch length C, some representative parameters were defined (extracted) from the response curve illustrated in Figure 6: the first starting angle θ_1, the first inflection point (bending moment resistance M_{p1}, angle

θ_{p1}), the first stiffness (the first gradient of moment M by θ) C_1, the tracking (rating) bending moment resistance M_{90} at $\theta = 90^{o}$, the second starting angle θ_2 (the reactional bending moment is zero when the folding angle is released), and the second stiffness C_2 at the second loading. Those parameters were measured for the normal and reverse folding directions, respectively.

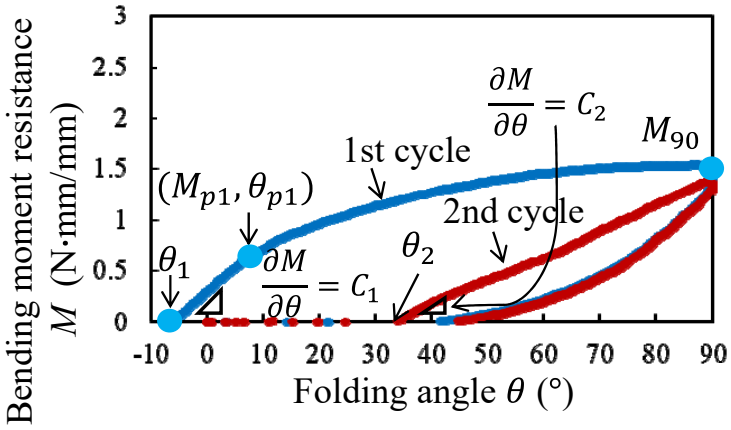

Figure 6. Example of the bending moment resistance M when varying the folding angle θ from θ_1 or θ_2 up to 90º, and the definition of representative parameters at the first cycle: θ_1, M_{p1}, θ_{p1}, M_{90}, C_1, and that at the second cycle θ_2, C_2 extracted from the response of M-θ. Herein, as the mechanical condition, the normal folding direction is chosen, the residual indentation depth is $d_{2as} = 1 - d_{2R}/t \approx 0.45$, and the plain-uniform trapezoidal blade (B = 30 mm) is selected as the example.

According to the previous report on the crease bending characteristics of a scored-0.3-mm-thick PP sheet [16], the interior scored contact interference was known from the bending moment resistance in the normal folding. However, the rating bending moment resistance M_{90} at 90º was not analyzed from aspects of dependency on the residual indentation depth d_{2as}/t. Some parameters, such as M_{p1}, C_1, M_{90} and C_2, were discussed using theoretical models of elastic-limitation and plastic collapse [20–22]. Since C_1, C_2 and resistance M_{p1} were mainly determined by the stress concentration effect at the scored notch, the indentation depth d_{2as}/t of the scored notch was recognized as a primary control parameter.

3. Results and discussions

3.1. Profile of scored PC sheet

Before discussing the bending moment resistance of Case 1 (variable pitch C under $d_{2as}/t = 1 - d_{2R}/t \approx 0.45$), ascertaining the relationship between the profile of the scored part and the residual indentation depth $1 - d_{2R}/t$ is convenient for understanding the contact interference of burrs or uncut layer at the bottom layer. Hence, the profiles of the scored part were first explained in Case 2 ($1 - d_{2R}/t$ = 0.25–0.75). Figures 7–9 show side views of the scored PP sheets when using the plain-uniform trapezoidal, 0.5 × 0.5 perforation and 3 × 3 perforation blades, respectively.

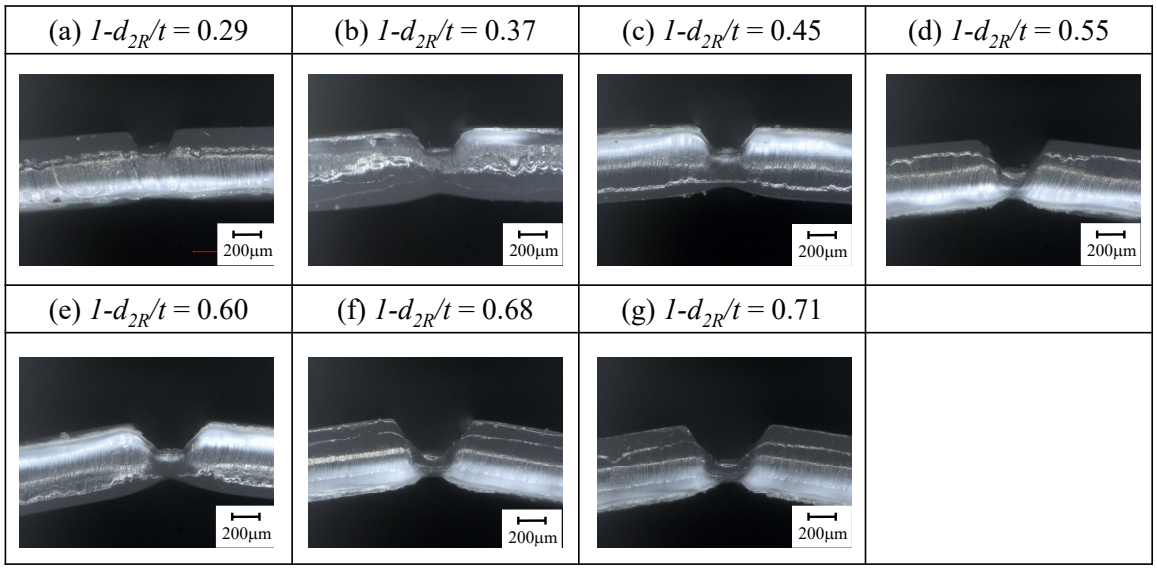

Figure 7. Side views of scored PP sheet using the plain-uniform blade (trapezoidal of 0.21-mm tip thickness), when choosing the normalized residual indentation depth as $d_{2as}/t = 1 - d_{2R}/t$ = 0.29, 0.37, 0.45, 0.55, 0.6, 0.68 and 0.71.

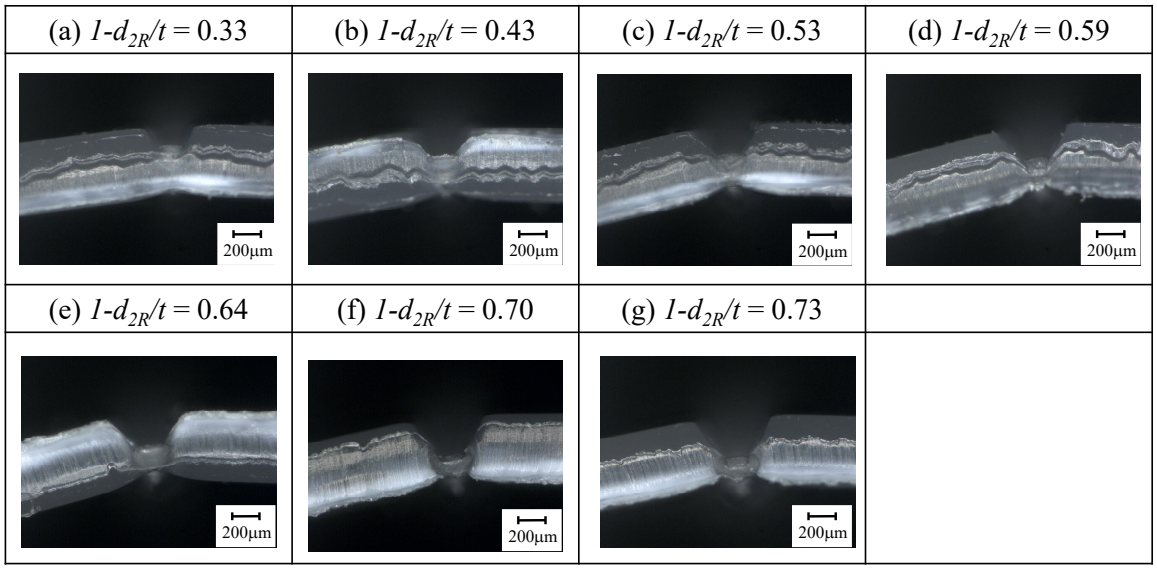

Figure 8. Side views of scored PP sheet using the 0.5 × 0.5 perforation blade, when choosing the normalized residual indentation depth as $d_{2as}/t = 1 - d_{2R}/t$ = 0.33, 0.43, 0.53, 0.59, 0.64, 0.70 and 0.73.

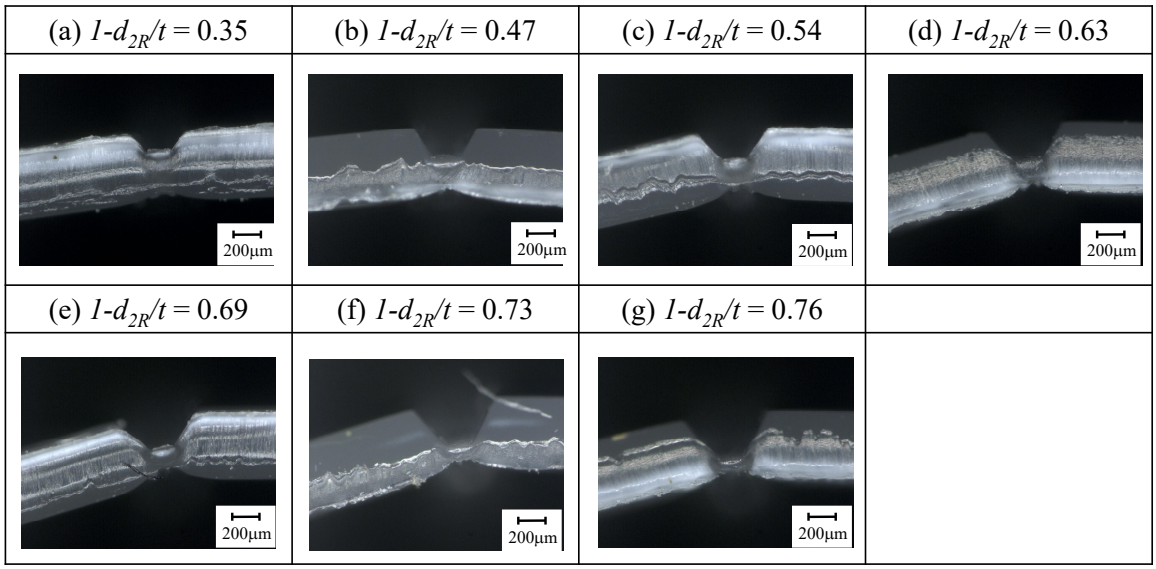

Figure 9. Side views of scored PP sheet using the 3 × 3 perforation blade, when choosing the normalized residual indentation depth as $d_{2as}/t = 1 - d_{2R}/t$ = 0.35, 0.47, 0.54, 0.63, 0.69, 0.73 and 0.76.

When $d_{2as}/t = 1 - d_{2R}/t > 0.43$–$0.47$, the bottom layer was remarkably necked at the scored zone, and the warp angle of the PP sheet was about 5º–15º for opening the wedged side (upper side). A narrow range of $d_{2as}/t = 1 - d_{2R}/t = 0.43$–$0.47$ was collected and used as Case 1. In the case of $d_{2as}/t = 1 - d_{2R}/t < 0.43$, as the cutting zone (part *A*) was cut off insufficiently, the creasing line comprised two kinds of half-cut grooves (parts *A* and *B*).

Figures 10 and 11 show the top (a) and back (b) views of scored the PP sheet when using the 0.5 × 0.5 perforation blade and the 3 × 3 perforation blade, respectively. The nicked part *B* (trapezoidal) was relatively spread out compared to the cutting part *A*, due to the plastic-compressive deformation flow by the trapezoidal tip profile of the blade. The cutting part *A* was kissed or interfered at the bottom layer for $d_{2as}/t = 1 - d_{2R}/t < 0.5$, whereas it was opened with a certain nonzero gap for $d_{2as}/t = 1 - d_{2R}/t > 0.5$. The width W_c of the cutting zone at part *A* was measured and arranged in Figure 12. The 3 × 3 perforation (Figure 12b) shows that the nonzero starting point was detected at $d_{2as}/t = 1 - d_{2R}/t = 0.5$. In this case, the nonzero condition matched $d_1/t > 1$ geometrically. When $d_{2as}/t = 1 - d_{2R}/t = 0.76$, the spread-out width was calculated as (0.76 mm − 0.5 mm) × 2tan21º = 0.1 mm, whereas the measured size of W_c was about 0.08 mm in Figure 12b. Hence, the difference of 0.1 − 0.08 mm = 0.02 mm was estimated as a shrinked width. The 0.5 × 0.5 perforation in Figure 12b showed that the measured W_c was about +0.02 mm larger than that of the 3 × 3 perforlation. Thus, the starting point of nonzero was about $d_{2as}/t = 1 - d_{2R}/t = 0.35$ in the case of the 0.5 × 0.5 perforation. Also, the interference of burrs or cutting over at the bottom layer was varied with pitch *C*.

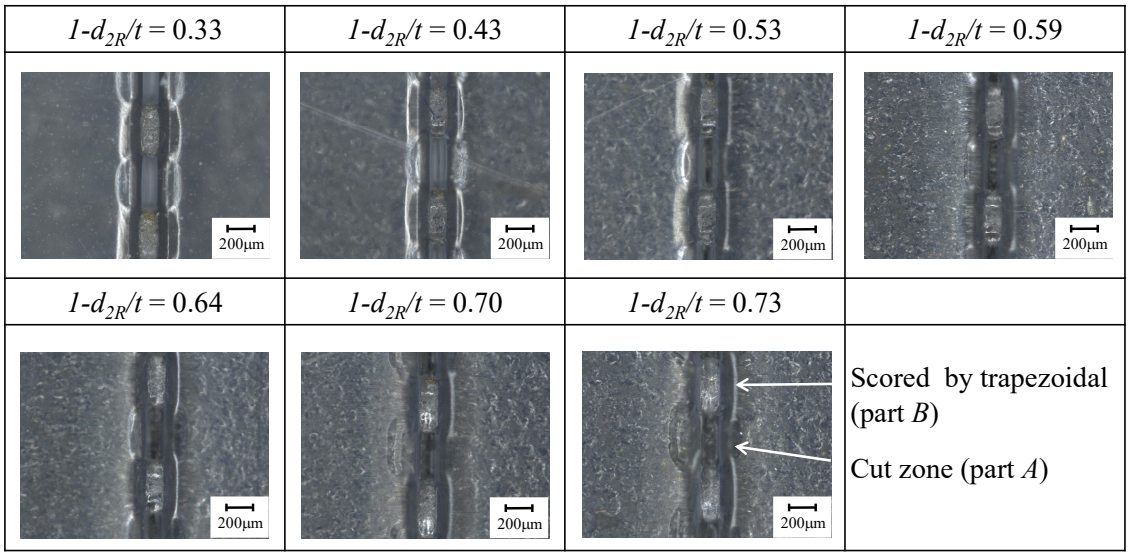

(a)

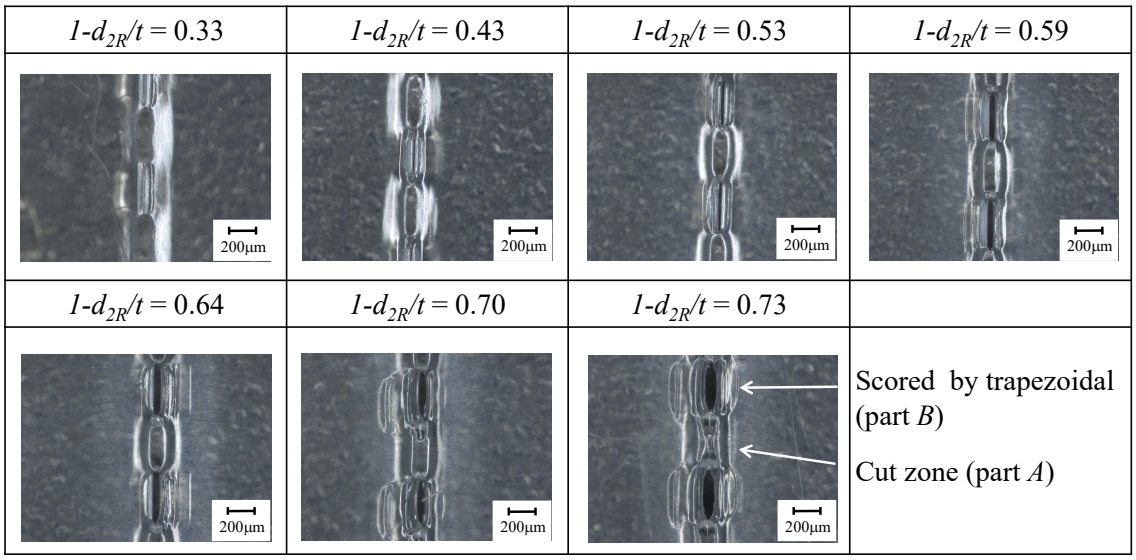

(b)

Figure 10. Top views of scored PP sheet using the 0.5 × 0.5 perforation blade, when choosing the normalized residual indentation depth as $d_{2as}/t = 1 - d_{2R}/t = 0.33$, 0.43, 0.53, 0.59, 0.64, 0.70 and 0.73. (a) Front side (scored side by a blade edge) and (b) back side (bottom side).

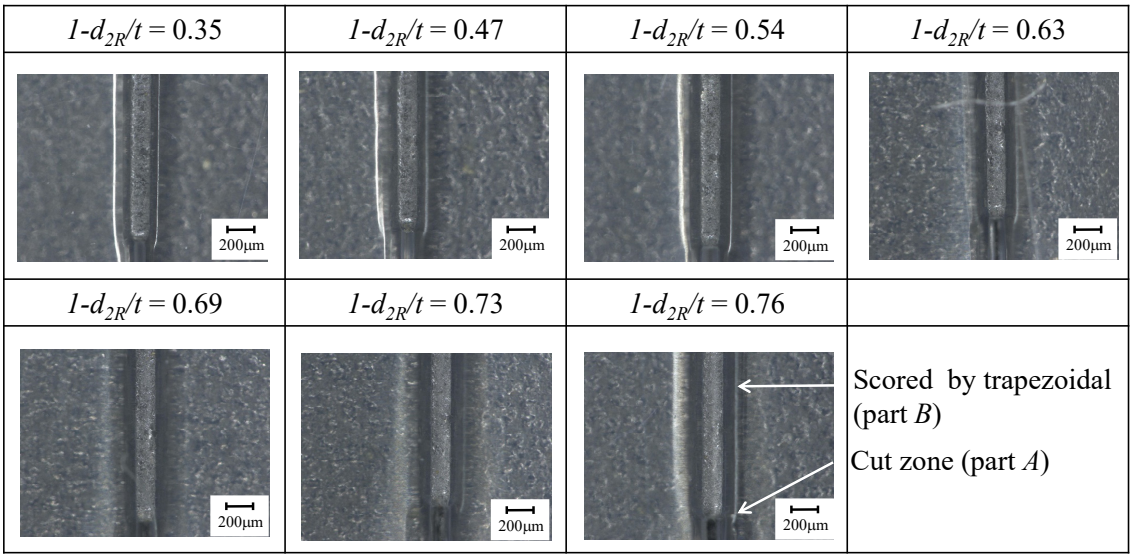

(a)

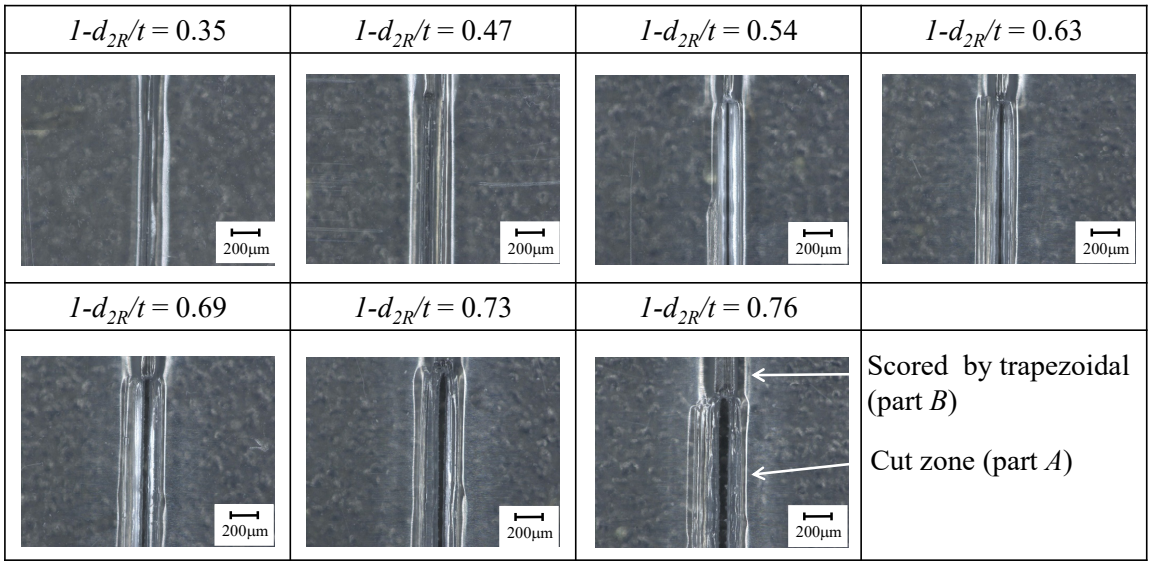

(b)

Figure 11. Top views of scored PP sheet using the 3 × 3 perforation blade, when choosing the normalized residual indentation depth as $d_{2as}/t = 1 - d_{2R}/t = 0.35$, 0.47, 0.54, 0.63, 0.69, 0.73 and 0.76. (a) Front side (scored side by a blade edge) and (b) back side (bottom side).

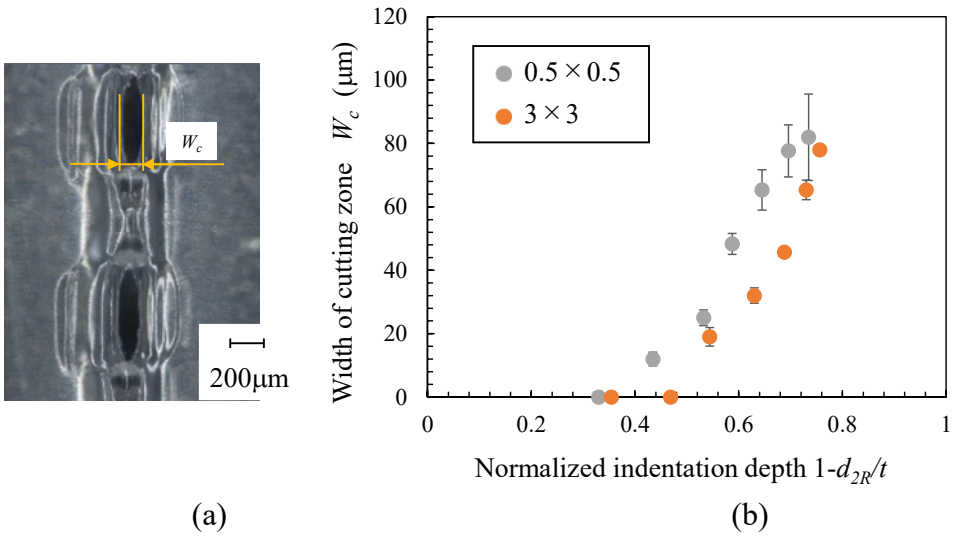

Figure 12. Dependency of width of cutting zone at part *A* on residual indentation depth at part *B*. (a) Spread-out width of cutting zone illustrated in a photograph of back view, and (b) relationship between width of cutting zone and normalized residual indentation depth.

3.2. Load response during scoring process

Before seeing the perforation load response, a new virgin blade and the plain-uniform trapezoidal blade of 0.21 mm tip thickness were examined in the cutting test of the 0.5 mm thickness PP sheet. Figure 13a,b show the relationship between the cutting line force $f = F/W$ and the normalized indentation depth d_1/t, d_2/t, when cutting the PP sheet by using the new virgin and the plain-uniform-trapezoidal blades, respectively.

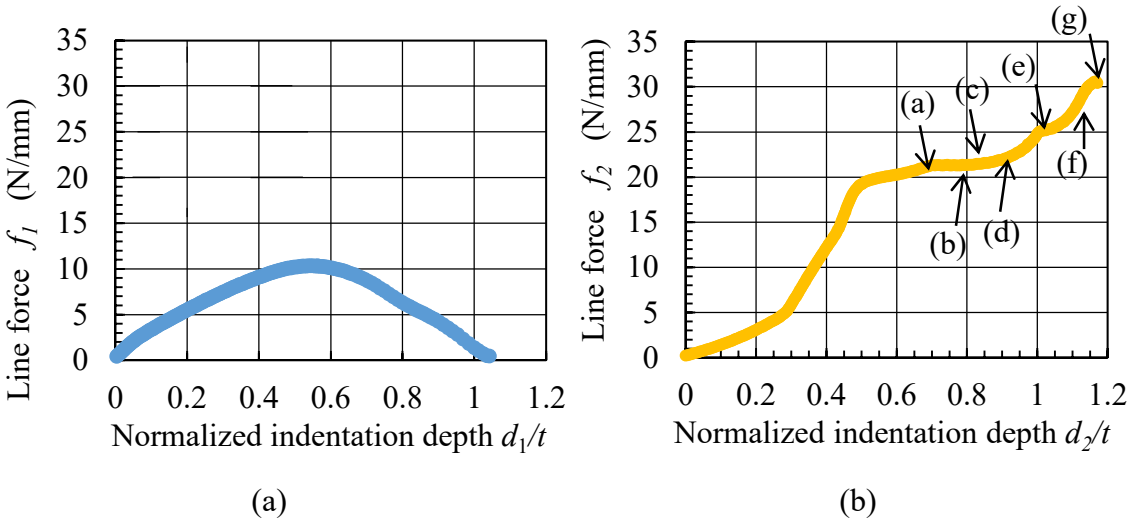

Figure 13. Relationship between the line force and the indentation depth of the blade holder. (a) Cutting by a new virgin blade, and (b) scoring (cutting) by a plain-uniform trapezoidal blade.

The maximum line force of the new virgin blade was about 10 N/mm at 50% of the thickness t = 0.5 mm, whereas the cutting load by the plain-uniform trapezoidal blade of the 0.21 mm tip thickness showed the yielding resistance of 20–22 N/mm for d_2/t = 0.5–0.9. The drawn tags (a)−(g) in Figure 13b corresponded deformation states shown in Figure 7. Since the state of (c) was $d_{2as}/t = 1 - d_{2R}/t$ = 0.45, the scoring line force of the plain-uniform trapezoidal blade was estimated at 22 N/mm in Case 1. So far, an equivalent maximum line force of the perforation blade was expected to be 0.5 × 10 + 0.5 × 20 = 15 N/mm, because $A = B = 0.5C$ was assumed with respect to the profile of the perforation blade. As the line force f_2 remarkably increased for $d_2/t > 1$ (including the displacement of underlay and holder device) (Figure 13b), to precisely control the residual indentation depth d_{2as} becomes difficult using a certain tip thickness of the trapezoidal blade. When considering only $d_2/t < 0.9$ ($d_{2as}/t < 0.5$), the scoring line force is stably estimated as being less than 22 N/mm. Therefore, the loading condition of Case 1 was recognized as a stable scoring state.

Figure 14 shows the relationship between the scoring line force $f = F/W$ and the normalized indentation depth d_1/t, when pushing the PP sheet by the six perforation blades chosen as C = 0.5, 1.0, 2, 4, 6, and 8 mm, respectively. The line force remarkably increased at d_1/t = 0.5–0.6 and culminated at d_1/t = 0.7–0.8. The former (remarkably increasing as a stepped response) was caused by the kissing and starting of the indentation of the nicked zone (part B), whereas the latter passed through the necking state of the cutting zone (part A).

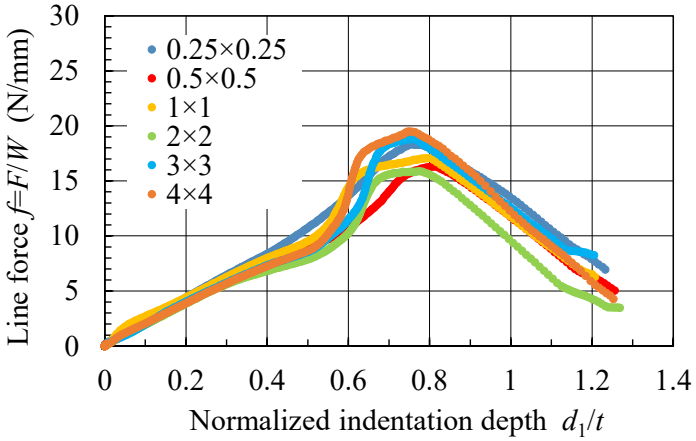

Figure 14. Relationship between the scoring (cutting) line force and the normalized indentation depth when using perforation blades chosen as C = 0.5, 1.0, 2, 4, 6, and 8 mm. Herein, the residual indentation depth was $d_{2as}/t = 1 - d_{2R}/t \approx 0.45$ when d_1/t reached 1.2–1.27.

Although the maximum line force varied with the pitch C, its tendency was not monotone with C. The former (remarkably increasing as a stepped response) was weakened and a smooth-peaked response when C < 1 mm (almost being the micro perforation). In Figure 14, the maximum line force was almost 15–20 N/mm, close but exceeded 15 N/mm. Hence, it was found that the prediction of combined cutting resistance from Figures 12 and 13 (described) was close, but slightly smaller than the real maximum peak values. This additional resistance in the real scoring process caused the generation of 3D cutting corners.

3.3. *Effects of pitch length on bending moment resistance*

The effects of the pitch length C on the bending moment resistance M were investigated in Case 1 ($d_{2as}/t = 1 - d_{2R}/t \approx 0.45$). Figure 15 shows the representative bending moment resistance M when folding from $\theta = \theta_1$ and $\theta = \theta_2$ to 90º (double folding) under a rotational velocity of $\omega = 0.2$ rps. The early stage ($\theta < 40$º) of the load response slightly varied with the pitch length. Also, when the bent inside of the scored zone (part B) had no interference, the rating bending moment M_{90} slightly varied for $C \geq 4$ mm. However, when $C \leq 2$ mm, the bent inside of the scored zone was kissed and the bending moment resistance remarkably increased for 50º < θ < 90º, whereas the bent inside of the scored zone had a certain clearance and the bending moment resistance almost saturated for 50º < θ < 80º when $C \geq 4$ mm.

Figure 16 shows two cases: (a) the scored inside was almost kissed state at $C = 1$ mm, and (b) the clearance existed at $C = 6$ mm, when the PP sheet was bent to $\theta = 70$º.

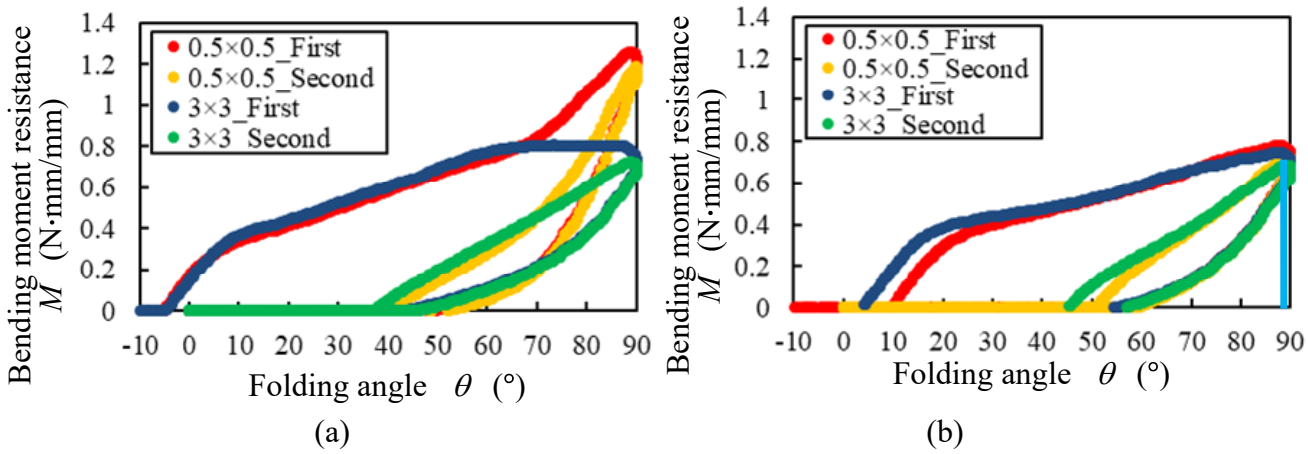

Figure 15. Relationship between the bending moment resistance M and the folding angle θ when varying θ from θ_1 to 90º at the first folding and θ from θ_2 to 90º at the second folding. Herein, the 0.5 × 0.5 and 3 × 3 perforation blades were used for scoring the residual indentation depth $d_{2as}/t = 1 - d_{2R}/t \approx 0.45$. (a) Normal and (b) reverse folding directions.

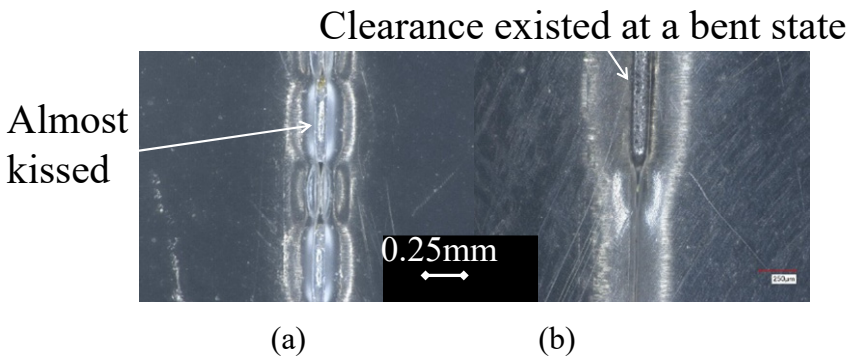

Figure 16. Top views of the bent inside of the scored zone at $\theta \approx 70$º. (a) $C = 1$ mm and (b) $C = 6$mm.

To characterize the bending moment resistance of the scored line, the bending moment at the first inflection M_{p1}, the rating bending moment M_{90} at $\theta = 90°$, the first and second stiffness values C_1 and C_2, and the second starting angle θ_2 were arranged with the pitch C. Figure 17 shows the bending moment resistance at the first inflection M_{p1} and its corresponded angle $\theta_{p1}-\theta_1$ when choosing the six perforation blades (C = 0.5, 1, 2, 4, 6 and 8 mm), and the plain-uniform trapezoidal blade. In Figure 17, blue and brown represent the normal and reverse folding directions, respectively. Since $M_{p1} \approx 0.3$ N·mm/mm in the normal/reverse directions at the six perforation blades, and $M_{p1} \approx 0.7$ N·mm/mm in the reverse direction at the plain-uniform trapezoidal blade, their ratio was about 0.43. Since $B/C = 0.5$, this result was reasonable, because the cutting part A was half of the width of the PP sheet. The difference between the normal and reverse folding directions was less than 20% of M_{p1} at the perforation blades, and less than 15% of M_{p1} at the plain-uniform trapezoidal blade. In the case of the plain-uniform trapezoidal blade, the normal M_{p1} was stably larger than the reverse M_{p1}. This trend was probably caused by the stress concentration effect at the scored notch.

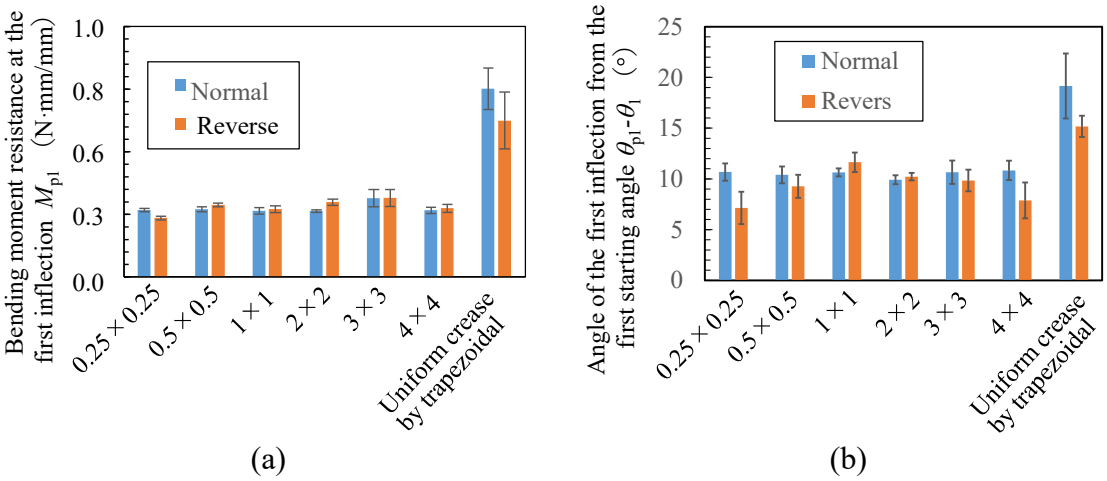

Figure 17. The first inflection (yield) point of the bending moment resistance when choosing the six perforation blades and the plain-uniform trapezoidal blade at $d_{2as}/t = 1$ $d_{2R}/t \approx 0.45$. (a) Bending moment resistance at the first inflection and (b) angle at the first inflection.

The occurrence of the inflection of the bending moment resistance at $\theta_{p1} - \theta_1 = 10°$–$20°$ was the same tendency as that of the previous report of a 0.3-mm-thick PP sheet by a two-line wedge knife [16]. According to the theory of plasticity [20–22], the bending moment resistance of a unit-width uniform beam at the elastic limitation was estimated as Eq 2, whereas that at the plastic collapse was estimated as Eq 3.

$$M_{el} = \sigma_Y (d_{2R})^2/6 \tag{2}$$

$$M_{pc} = \sigma_Y (d_{2R})^2/4 \tag{3}$$

Substituting $\sigma_Y = 31.9$ MPa (the tensile yielding stress from Table 1), and $d_{2R} = 0.275$ mm (the residual height of scored zone) into Eqs 2 and 3 gives $M_{el} = 31.9 \times 0.275 \times 0.275/6 = 0.4$ N·mm/mm, and $M_{pc} = 6M_{el}/4 = 0.6$ N·mm/mm, respectively.

When considering the perforation state of a scored line at B/C = 0.5, the expected bending moment resistance was just half of the plain-uniform scored model, because no bending resistance was assumed at the cutting zone. Hence, the expected resistances are $0.5M_{el}$ = 0.2 N·mm/mm and $0.5M_{pc}$ = 0.3 N·mm/mm at the six perforation blades. So far, the bending moment resistances of the elastic limitation and plastic collapse were estimated as 67% and 100% of the experimental M_{p1} (0.3 N·mm/mm) at the six perforation blades, respectively. They were also estimated as 57% and 86% of the experimental M_{p1} (0.7 N·mm/mm) at the plain-uniform trapezoidal blade, respectively. Therefore, the inflection point was mainly caused by the yielding collapse or the plastic bending behavior of the scored zone.

Using Eq 1 and Figure 17, the strain rate of bending deformation at the scored notch is calculated. Watching the uniform crease, as M_{p1} = 0.7 N·mm/mm, θ_{p1} = 20º, ω = 0.2 × 360º/s, the bending strain rate $\dot{\varepsilon}_b$ was estimated as 0.16 s^{-1}. This folding deformation seems to be a brittle state.

Figure 18 shows the rating bending moment resistance at a folding angle of 90º in the normal and reverse folding directions when using the six perforation blades and the plain-uniform trapezoidal blade for scoring. Herein, the residual indentation depth was set as $d_{2as}/t = 1 - d_{2R}/t \approx 0.45$. Considering the reverse folding, $M_{90} \approx$ 0.7 N·mm/mm at the six perforation blades whereas $M_{90} \approx$ 1.4 N·mm/mm at the plain-uniform trapezoidal blade, and then the ratio of the former to the latter was 0.5. This trend was reasonable due to the geometrical relation B/C = 0.5.

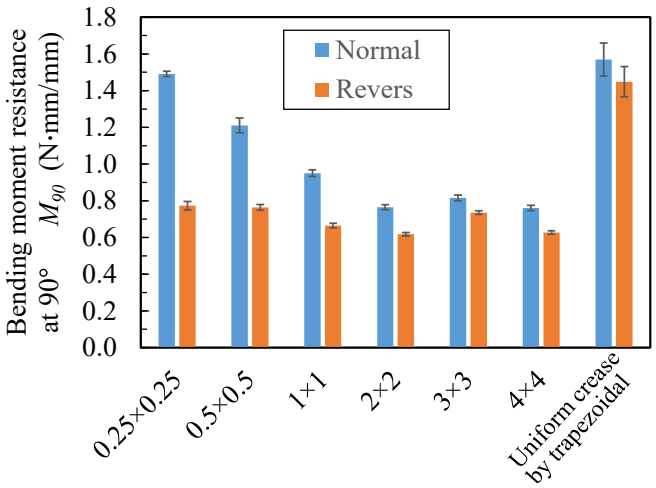

Figure 18. Rating bending moment resistance M_{90} at θ = 90º when choosing the six perforation blades and the plain-uniform trapezoidal blade at $d_{2as}/t = 1 - d_{2R}/t \approx 0.45$.

The normal folding M_{90} remarkably increased for 0.5 mm < C < 2 mm, whereas the reverse folding M_{90} was almost constant for 0.5 mm < C < 8 mm. This increment in the normal folding M_{90} was detected for θ > 50º–70º (Figure 15a), and its mechanism was confirmed as an interior scored kissing (Figure 16). When the interior scored kissing disappeared for the perforation blades ($C \geq$ 4 mm) and the plain-uniform trapezoidal blade, the normal folding M_{90} was +0.1 N·mm/mm larger than the reverse folding M_{90}. This small difference of 0.1 N·mm/mm was probably caused by the contact interference of the scored inside.

As for the 90º folding, the bending stress seems to be in the plastic collapse state. Although M_{90} can be predicted as $\sigma_Y (d_{2R})^2/4$, since the yield stress increases by the work hardening, the plastic collapse bending moment is $\sigma_{Y90} (d_{2R})^2/4$. Here, for example, when σ_{Y90} is assumed to be σ_B = 42.1 MPa, then M_{pc} = 42.1 × 0.275 × 0.275/4 = 0.8 N·mm/mm. In the reverse folding, since $M_{90} \approx$ 1.4 N·mm/mm in the experiment, this assumption was insufficient. Due to the work hardening and the large deformation, σ_{Y90} appeared to be $(1.4/0.8)\sigma_B = 1.75\sigma_B$ = 73.7 MPa.

Evidently, the relative crease strength was well predicted from the design theory of plasticity.

Figure 19a,b show the first and second stiffnesses values (gradients of the bending moment resistance) C_1 and C_2 at the first and second starting angles θ_1 and θ_2 in the normal and reverse folding directions, respectively, when using the six perforation blades and the plain-uniform trapezoidal blade for scoring. The residual indentation depth was set as $d_{2as}/t = 1 - d_{2R}/t \approx 0.45$. Considering the normal folding, $C_1 \approx 0.03$ N·mm/mm/º when using the six perforation blades, whereas $C_1 \approx 0.045$ N·mm/mm/º when using the plain-uniform trapezoidal blade. Also, the ratio of the former to the latter was 0.67. This value should be theoretically 0.5 because the cutting part A is expected to experience no bending moment. Hence, the cutting part A excessively increases the bending stiffness in the folding process. This trend is probably caused by some contact interference of burrs or a thin uncut layer at the cutting part A (Figure 4a,b).

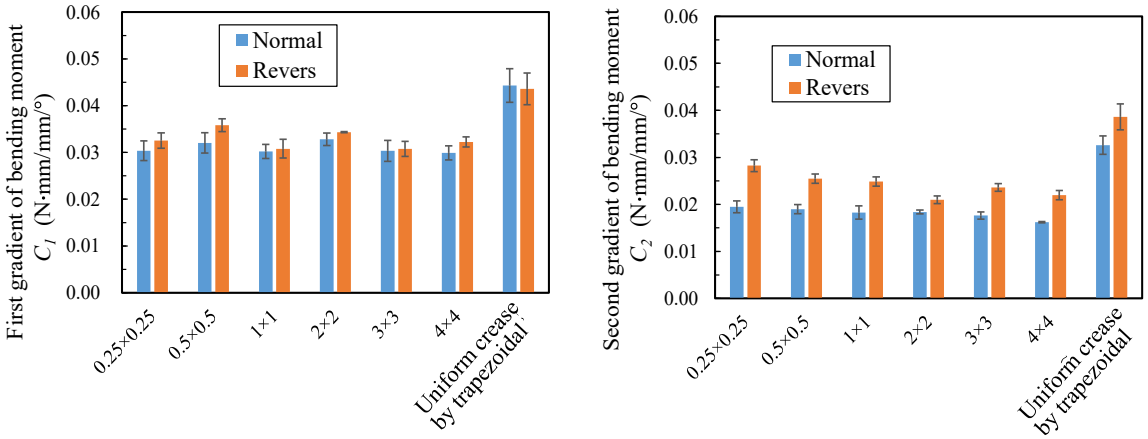

Figure 19. Comparison of the gradient of bending moment resistance when choosing the six perforation blades and the plain-uniform trapezoidal blade at $d_{2as}/t = 1 - d_{2R}/t \approx 0.45$. (a) First gradient of bending moment resistance at $\theta = \theta_1$, and (b) second gradient of bending moment resistance at $\theta = \theta_2$.

Similarly, considering the second normal folding, $C_2 \approx 0.018$ N·mm/mm/º when using the six perforation blades, whereas $C_2 \approx 0.033$ N·mm/mm/º when using the plain-uniform trapezoidal blade. The ratio of the former to the latter is 0.55. This value is relatively close to the theoretical value of 0.5.

In the reverse folding, the first stiffness C_1 slightly differed from that of the normal folding, whereas the second stiffness C_2 was stably slightly larger (0.005–0.01 N·mm/mm/º) than that of the

normal folding. This difference in C_2 between the normal and reverse folding is probably due to the stress concentration and the work hardening at the outside surface layer.

Figure 20 shows the second starting angle θ_2 in the normal and reverse folding directions when using the six perforation blades and the plain-uniform trapezoidal blade. The reverse folding θ_2 was 5º–10º larger than that of the normal folding. This trend indicates that the spring back in the normal folding exceeds that in the reverse folding. Then, the reverse folding generated larger plastic deformation at the scored zone in the folding process compared to the normal folding. This tendency of θ_2 seemed to be caused by the same reason responsible for the difference in C_2 between the normal and the reverse folding. The stress concentration and the local plastic deformation appeared to be larger/stronger on the outside surface at the scored zone under the reverse folding.

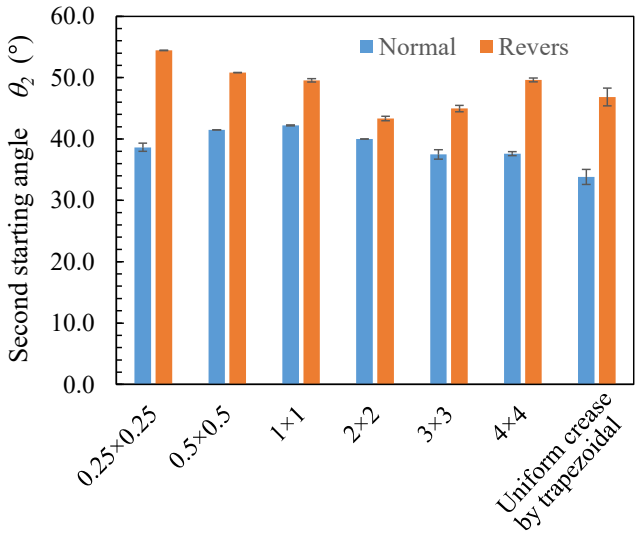

Figure 20. Second starting angle in the normal and reverse folding directions when choosing $d_{2as}/t = 1 - d_{2R}/t \approx 0.45$.

Figure 20 showed that the difference in θ_2 between the normal and the reverse folding was not even with the pitch C. The 2 × 2 perforation (C = 4 mm) had the minimum difference, whereas the 0.25 × 0.25 and 4 × 4 perforations had relatively larger differences. This tendency is similar to the difference in (θ_{1p}–θ_1) between the normal and the reverse folding (Figure 17b). This trend is a sort of positive correlation. Because when the angle of (θ_{1p}–θ_1) is smaller, the plastic deformation starts in the earlier position against the bending moment. This phenomenon is principally caused by the high-stress concentration at the bent surface of the scored PP sheet. Consequently, the spring back as 1 − θ_2/90º appears to become smaller (θ_2 increases) when the stress concentration is larger at the bent surface.

When choosing C = 0.5 mm (C/t = 1), the first stiffness C_1 and the bending moment resistance at first inflection M_{p1} were almost equal (considerably reducing the bending moment resistance) to that of the other perforation (1 mm < C < 8 mm) in the normal folding, whereas the rating bending moment M_{90} was almost equal (having a large resistance against the final folding) to that of the plain-uniform trapezoidal blade in the normal folding. Hence, the microperforation (C/t < 1.7) appears to perform differently, compared to others (C/t > 2).

3.4. Effects of indentation depth on bending moment resistance

As previously reported [16], as the residual indentation depth $d_{2as}/t = 1 - d_{2R}/t$ increases, the representative three quantities M_{p1}, C_1 and C_2 decrease. When evenly combining the scored zone (part *B*) and the cutting zone (part *A*) as $B/C = A/C = 0.5$, these quantities should be half that of the plain-uniform trapezoidal blade, because the cutting part *A* is expected to experience no bending moment. However, as described in Section 3.3, the first and second stiffnesses C_1 and C_2 varied with the pitch *C*, and they were not always half that of the plain-uniform trapezoidal blade. Therefore, C_1 and C_2 were investigated here in the condition of Case 2: two kinds of perforation and plain-uniform trapezoidal were used in the range of $0.25 < 1 - d_{2R}/t < 0.75$.

Figure 21 shows the dependency of the first stiffness C_1 on the normalized residual indentation depth at the normal and reverse folding directions.

$$C_1 = -0.0537(1 - d_{2R}/t) + 0.0703 \quad \text{(for normal)} \tag{4}$$

$$C_1 = -0.0613(1 - d_{2R}/t) + 0.076 \quad \text{(for reverse)} \tag{5}$$

Here, Eqs 4 and 5 are the linear approximation derived from the experimental results of the plain-uniform trapezoidal blade. The ratio of Eq 5 to Eq 4 was about 1.08 for $0.25 < 1 - d_{2R}/t < 0.75$. When the residual indentation depth is shallow ($1 - d_{2R}/t < 0.2$), the stiffness C_1 saturates. The upper bound of C_1 is confirmed using the following discussion when the indentation depth is shallow. Regarding the first stiffness C_1, an elementary theory of a cantilever model is useful for determining the order of C_1 as the upper-bound [23,24]. Assuming that Young's modulus: $E = 1.25$ GPa (from Table 1), the span length: $\ell = 10$ mm, the second moment of area per unit width: $I = t^3/12$, and the height (thickness) of beam: $t = 0.5$ mm, the upper-bound stiffness per unit width C_{1UB} is estimated as the deflected angle of the cantilever (Eq 6). Herein, the unit of the rotation is considered as radian.

$$C_{1UB} = 2EI/\ell = Et^3/(6\ell) \tag{6}$$

Using the assumptions described above, C_{1UB} is calculated as $1250 \times 0.5^3/(6 \times 10) \times 3.14/180 = 0.045$ N·mm/mm/º. Figure 21 shows that the plots of the plain-uniform trapezoidal were slightly exceeded 0.045 N·mm/mm/º for $1 - d_{2R}/t < 0.4$. The value of *E* should be updated in a bending mode test. Also, note that the linearization of Eqs 4 and 5 was limited in the specified range: $0.25 < 1 - d_{2R}/t < 0.75$.

A virtual line of 0.5 × Eq 4 and that of 0.5 × Eq 5 are drawn in Figure 21a,b, respectively. Here, "0.5 × Equation" indicates that a half value of the Equation was calculated. These lines correspond to the stiffness of part *B* (scored zone).

Figure 21a shows that the stiffness C_1 with the perforation ($C = 1$ mm, 6 mm) at the normal folding is almost linear between the upper line of Eq 4 and the lower line of 0.5 × Eq 4. Similarly, Figure 21b shows that the stiffness C_1 with the perforation ($C = 1$ mm, 6 mm) at the reverse folding is almost linear relationship between the upper line of Eq 5 and the lower line of 0.5 × Eq 5. The stiffnesses C_1 with the two perforations are close to the upper line Eqs 4 and 5 for $1 - d_{2R}/t < 0.3$, whereas they are quite close to the lower line 0.5 × Eqs 4 and 5 for $d_{2as}/t = 1 - d_{2R}/t > 0.7$. When choosing $d_{2as}/t = 1 - d_{2R}/t \approx 0.45$, $C_1 \approx 0.7$–0.75 × Eqs 4 and 5. This result almost matches Figure 19. Also, Figure 12 shows that the width of the cutting zone W_c is nonzero for $d_{2as}/t = 1 - d_{2R}/t > 0.5$, and C_1 is pretty close to the lower line 0.5 × Eqs 4 and 5. So far, the contact interference

of burrs at the cutting bottom layer disappears for $d_{2as}/t = 1 - d_{2R}/t > 0.7$, and at that time, C_1 is almost half of that of the plain-uniform trapezoidal blade.

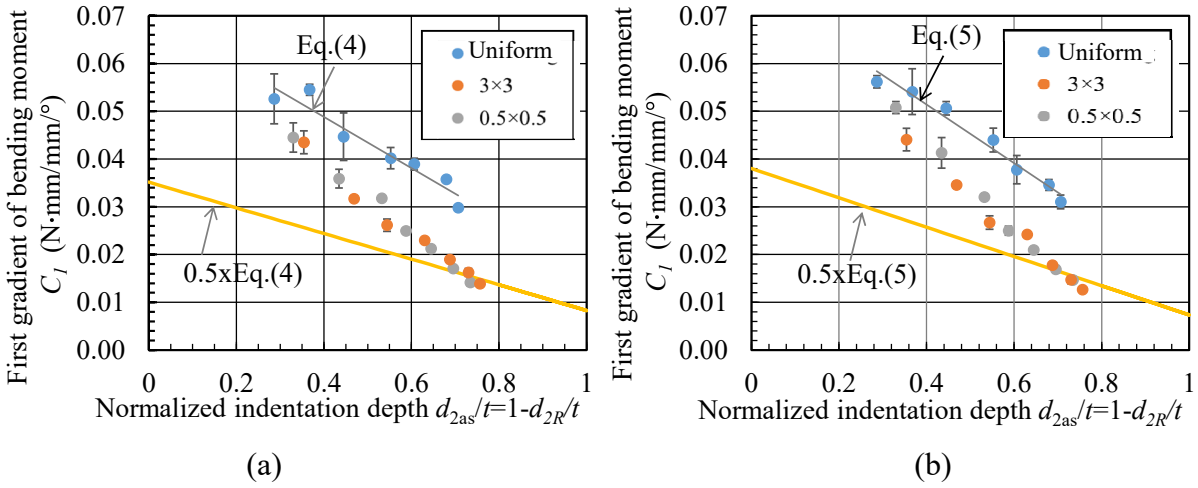

Figure 21. Relationship between the first stiffness (gradient of bending moment resistance) and the normalized indentation depth when using the perforation blade of C = 1 mm and 6 mm, and plain-uniform trapezoidal blade. (a) Normal and (b) reverse folding directions.

Figure 22 shows the dependency of the second stiffness C_2 on the normalized residual indentation depth at the normal and reverse folding directions. Here, Eqs 7 and 8 are the linear approximations derived from the experimental results of the plain-uniform trapezoidal blade. The ratio of Eq 8 to Eq 7 was about 1.1–1.7 for $0.25 < 1 - d_{2R}/t < 0.75$. Evidently, the reverse had a larger stiffness than the normal. Considering the ratios of Eq 4/Eq 7 and Eq 5/Eq 8, C_2 was about 70%–80% of C_1 in the case of the plain-uniform trapezoidal blade. Concerning the perforation blades, C_2 was almost linear between the upper line of Eq 7 and the lower line of 0.5 × Eq 7 at the normal folding direction. Also, it was almost a linear relationship between the upper line of Eq 8 and the lower line of 0.5 × Eq 8 in the reverse folding direction, respectively. Here, C_2 was close to the lower lines (Figure 22). Namely, through the first folding cycle up to 90º, some contact interference of burrs and/or the thin uncut layer at the cutting zone (part A) appears to be plastically weakened.

$$C_2 = -0.056(1 - d_{2R}/t) + 0.0587 \quad \text{(for normal)} \tag{7}$$

$$C_2 = -0.0472(1 - d_{2R}/t) + 0.0617 \quad \text{(for reverse)} \tag{8}$$

As described in Section 3.3, the first inflection of the bending moment resistance M_{p1} (Figure 17) was discussed using the plastic collapse by Eq 3 when choosing $d_{2as}/t = 1 - d_{2R}/t \approx 0.45$. To estimate the M_{p1} behavior when changing $d_{2as}/t = 1 - d_{2R}/t = 0.25$–$0.75$, the relationship between M_{p1} and d_{2as}/t was investigated using two perforation blades (C = 1 mm, 6 mm) and the plain-uniform trapezoidal blade for the normal and reverse folding directions (Figure 23). According to the previous report [16], M_{p1} was linearly approximated with d_{2R}/t, although the plastic collapse model was partially discussed [20–22]. Obviously, the second order polynomial with d_{2R}/t: Eq 3 and 0.5 × Eq 3 well explains the amplitude of M_{p1}.

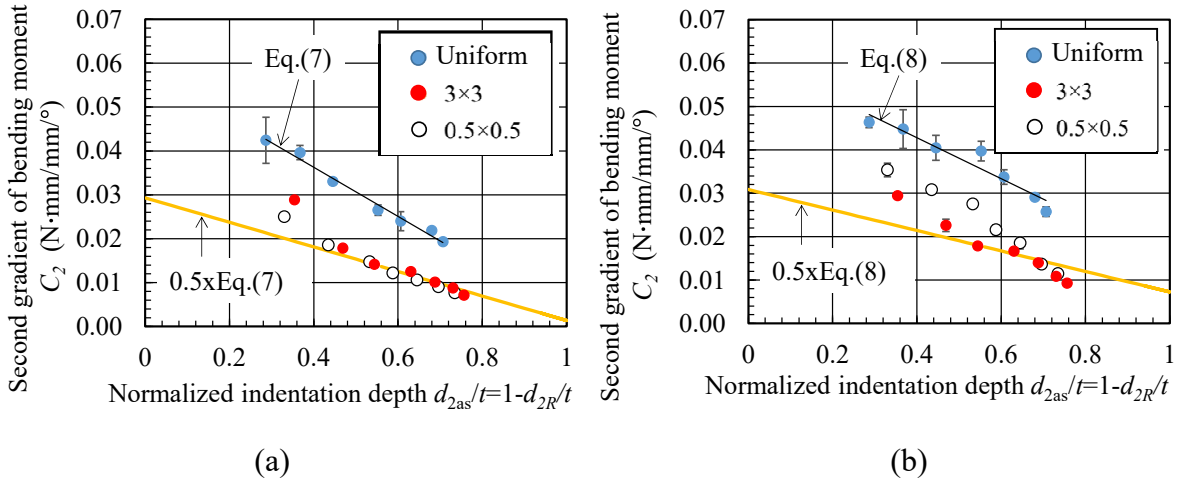

Figure 22. Relationship between the second stiffness (gradient of bending moment resistance) and the normalized indentation depth when using the perforation blade of C = 1 mm and 6 mm, and plain-uniform trapezoidal blade. (a) Normal and (b) reverse folding directions.

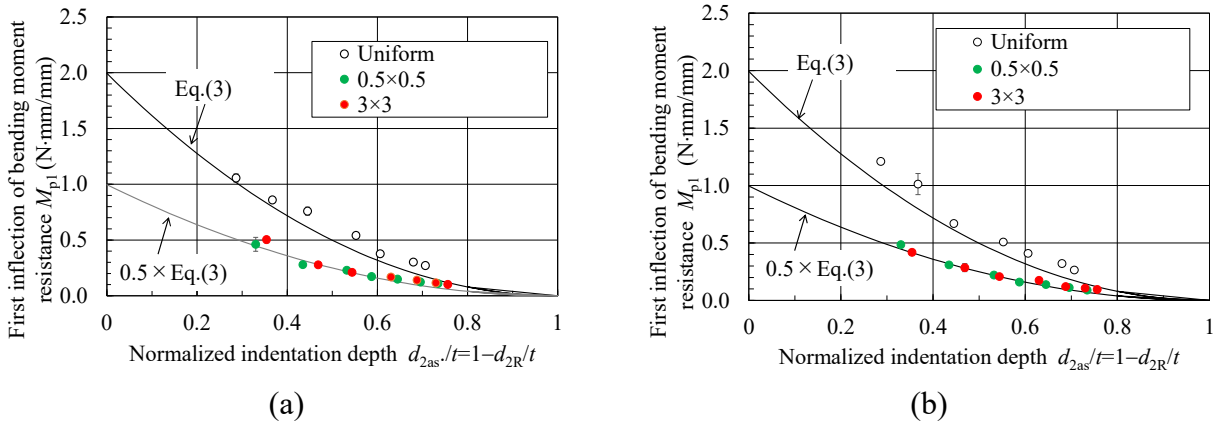

Figure 23. Dependency of the first inflection of the bending moment resistance on the normalized residual indentation depth, (a) Normal and (b) reverse folding directions.

Regarding the rating bending moment resistance at θ = 90º (Figures 15 and 16), since there was a sort of interior kissing of the scored zone in the normal folding, an additional increase in the bending moment resistance occurred at θ > 50º–70º and $C \leq 2$ mm in the normal folding. Also, the work hardening, and/or contact interference at the scored zone, was remarkable when choosing $d_{2as}/t = 1 - d_{2R}/t \approx 0.45$.

To estimate the behavior of M_{90} when changing $d_{2as}/t = 1 - d_{2R}/t$ = 0.25–0.75, the relationship between M_{90} and d_{2as}/t was investigated using two perforation blades (C = 1 mm, 6 mm), and the plain-uniform trapezoidal blade for the normal and reverse folding (Figure 24). Henceforth, the yield stress was assumed to be $\sigma_{Y90} = 1.75\sigma_B$ = 73.7 MPa in Eq 3. Considering the reverse folding of Figure 24b, the experimental M_{90} of the plain-uniform trapezoidal blade matched Eq 3, whereas that

of the perforation blades (C = 1 mm, 6 mm) matched 0.5 × Eq 3. Therefore, the assumption of $\sigma_{Y90} = 1.75\sigma_B$ based on Eq 3 (a plastic collapse model) is reasonable and useful for predicting the bending moment resistance of scored PP sheets in the reverse folding.

In contrast, considering the normal folding in Figure 24a, in a shallow range of $d_{2as}/t = 1 - d_{2R}/t \leq 0.45$, the experimental M_{90} is partially predictable using the upper line of Eq 3 and the lower line of 0.5 × Eq 3. However, there were several kinds of unmatched behavior to Eq 3 and 0.5 × Eq 3. First, the experimental M_{90} of the perforation of C = 1 mm was close to that of the plain-uniform trapezoidal and larger than Eq 3 when $d_{2as}/t = 1 - d_{2R}/t > 0.45$. This trend was due to the additional increase in the bending moment resistance for θ > 50º–70º. Some contact interference at the scored zone appeared to increase the bending resistance. Second, the experimental M_{90} of the perforation of C = 6 mm was about 70% of that of the plain-uniform trapezoidal blade when $d_{2as}/t = 1 - d_{2R}/t >$ 0.45. Some contact interference characteristics at the scored zone increased the bending resistance for θ > 80º – 90º.

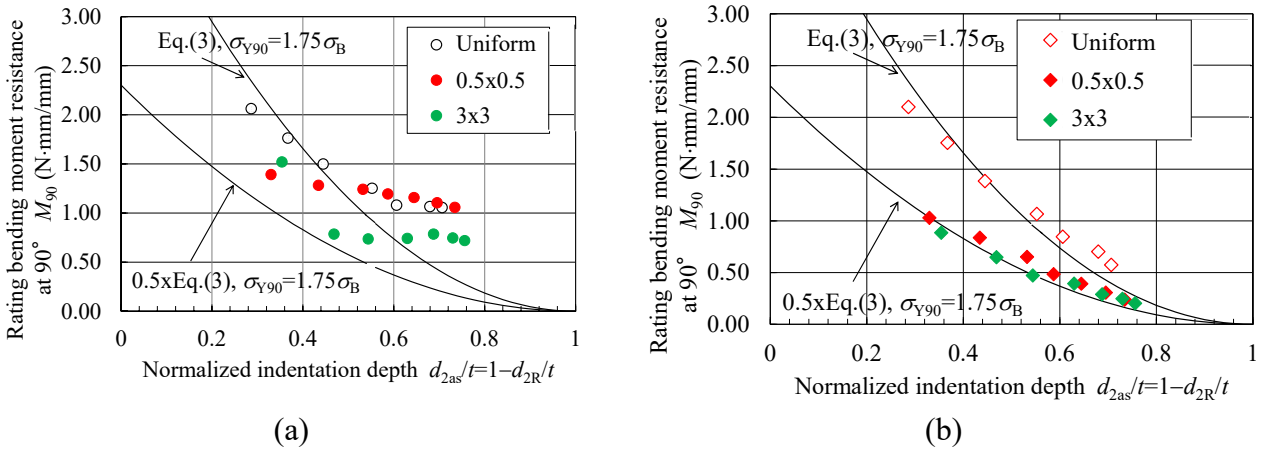

Figure 24. Relationship between the rating bending moment resistance at 90º and the normalized residual indentation depth. (a) Normal and (b) reverse folding directions.

Synthetically, the rating bending moment resistance M_{90} of perforation in the normal folding was unpredictable from some elementary theories for θ > 50º, because the contact interference often occurs at the scored zone (part B). However, the bending moment resistance at the inflection point M_{p1} is easily predictable from Eq 3, whereas the first stiffness C_1 is experimentally predictable as a linear relation, which is an intermediate resistance between the plain-uniform trapezoidal model and its 50% model. In the reverse folding, M_{90} is predictable using the modified Eq 3 and $\sigma_{Y90} = 1.75\sigma_B$, although M_{90} remarkably decreases when $d_{2as}/t = 1 - d_{2R}/t > 0.45$.

Figure 25 shows the second starting angle θ_2 when changing the residual indentation depth $d_{2as}/t = 1 - d_{2R}/t$ for two kinds of perforation blade (C = 1 mm, 6 mm) and the plain-uniform trapezoidal blade. The normal folding θ_2 was almost constant with $d_{2as}/t = 1 - d_{2R}/t$, whereas the reverse folding θ_2 increased with $d_{2as}/t = 1 - d_{2R}/t$. Also, the reverse folding θ_2 exceeded the normal folding θ_2. Comparing the three patterns (perforation), Figure 25 indicates that the fine pitch perforation (C = 1 mm) decreases the spring back (namely, it increases θ_2) in a folding process up to 90º.

Figures 24 and 25 reveal that the deep indentation of the scored zone (part B) contributes to the plastic collapse at the reverse folding of the scored zone, whereas it (deep indentation) accumulates

the elastic energy of the contact interference of the scored zone (part *B*). Also, M_{90} does not decrease with $d_{2as}/t = 1 - d_{2R}/t > 0.5$.

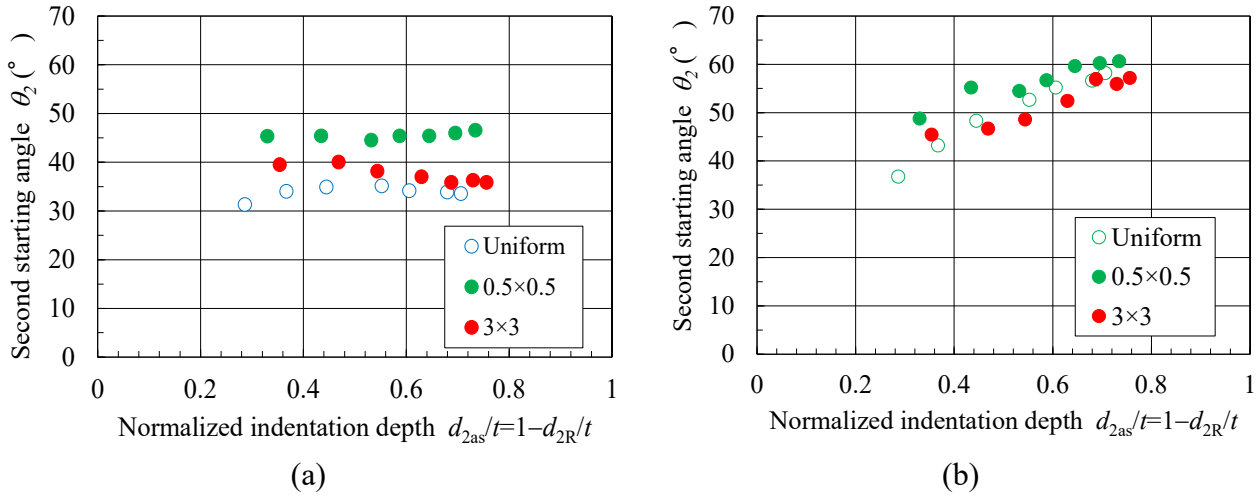

Figure 25. Relationship between the second starting angle and the normalized residual indentation depth for two perforation blades and the plain-uniform trapezoidal blade. (a) Normal and (b) reverse folding directions.

3.5. Bent profiles of perforation creasing line

In the bending test by CST-J1, it was challenging to take some bent profiles of desirable scored zones of the scored PP sheet, especially for $C < 2$ mm. Therefore, some bent profiles of the creasing line were overviewed manually. Figure 26 shows representative general views of bent corners concerning three scored-0.5-mm-thick PP sheets for the normal and reverse folding directions. These specimens were bent from θ_1 to 180º (making a sharp-folding form) and released in a natural, free state. Maintaining a certain bent state again, these bent corners were manually captured by a digital microscope. The specimens were smoothly bent without any cutting-off in the folding motion.

The following features were detected in the images: (i) In the reverse folding, the outside surface of the scored zone was smoothly or continuously cracked with a certain depth in the thickness direction (not split), whereas there was not any large propagation of cracks along the creasing line (in the lateral direction). (ii) In the normal folding, the scored zone was stably kissed at the inside when $\theta > 50$º and the outside was smoothly elongated and rounded. There was no propagation of cracks along the creasing line (in the lateral direction).

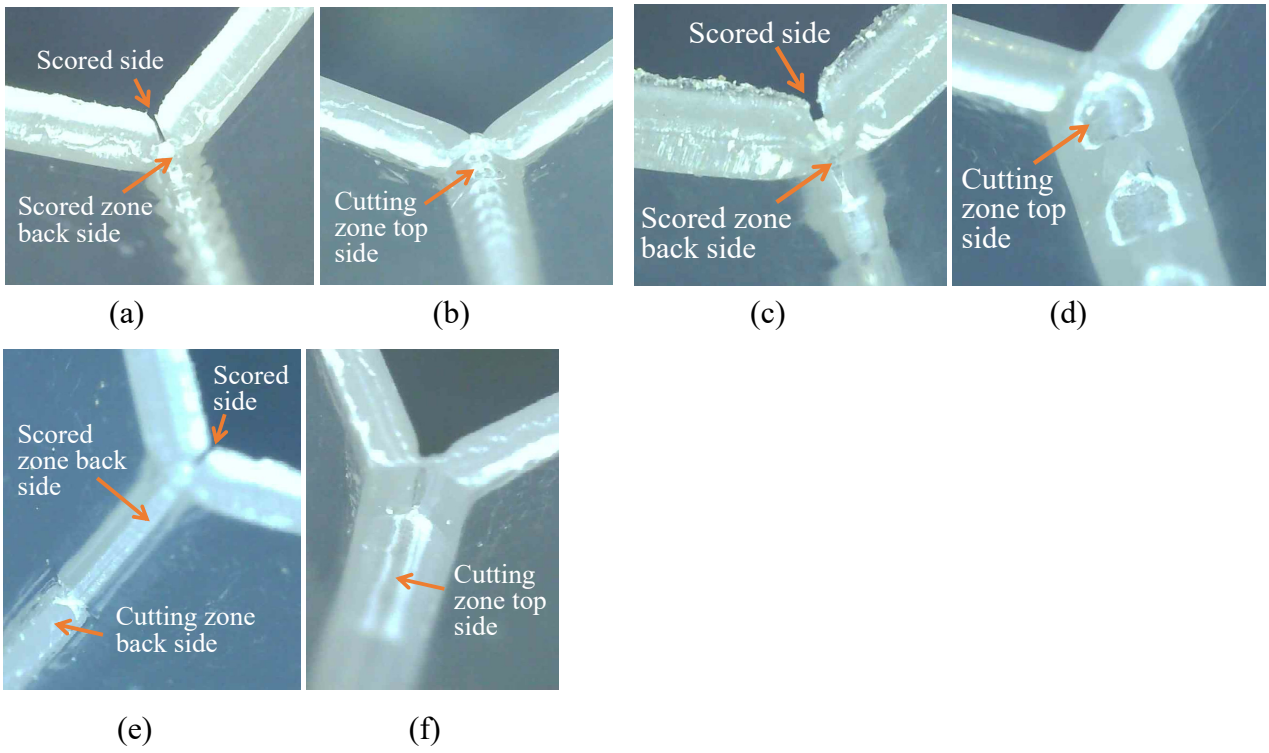

Figure 26. General views of bent crease line at $d_{2as}/t = 1 - d_{2R}/t \approx 0.45$ after folding up to 180º. (a) Normal folding at $C = 0.5$ mm, (b) reverse folding at $C = 0.5$ mm, (c) normal folding at $C = 1$ mm, (d) reverse folding at $C = 1$ mm, (e) normal folding at $C = 6$ mm and (f) reverse folding at $C = 6$ mm.

4. Conclusions

To reveal the crease bending characteristics of 0.5-mm-thick PP sheet using some perforation blades in the normal and reverse folding, the effects of an even combination of sharp and nicked-trapezoidal wedge blades on the scoring load response and bending moment resistance at the scored creasing line were experimentally investigated with several perforation-pitch lengths. As the crease bending characteristics, the first and second stiffnesses (gradient of bending moment resistance by folding angle) C_1 and C_2, the rating bending moment resistance at the right angle ($\theta = 90°$) M_{90}, the bending moment resistance at the first inflection point M_{p1}, and its corresponding angle θ_{p1} were discussed concerning the residual indentation depth of the blade against the PP sheet. Through this experiment, the following results were revealed.

(1) When changing the pitch length C of the perforation, the scoring force response remarkably changed at the first half process. When the nicked trapezoidal blade indented the PP sheet in the case of $C \geq 2$ mm, the load response had a stepped increase, whereas the sharp blade indented the PP sheet in advance (by $D = 0.25$ mm) and made a monotone increasing response. However, in the case of $C \leq 1$ mm, the load response showed a seamless (not any stepped) increasing response. The peak maximum scoring force of perforation exceeded the arithmetic mean of the sharp uniform wedge and the corresponding scoring force of the uniform nicked (trapezoidal) wedge.

(2) When changing C and keeping the normalized residual indentation depth $d_{2as}/t = 1 - d_{2R}/t \approx 0.45$, the response of the bending moment resistance M was not significantly changed with the normal and reverse folding in the early stage ($\theta < 40^{o}$), whereas it differed remarkably at the latter half ($50^{o} < \theta < 90^{o}$) between the normal folding and the reverse folding. When $C \leq 2$ mm, the bending moment resistance remarkably increased for $50^{o} < \theta < 90^{o}$ in the normal folding, due to the contact interference of the scored zone. In the scoring process of the perforation, as the wedged width of the cutting part increased with C, the scored width of the scored part was also affected by C, and then the bending moment resistance increased significantly in the latter half, especially for $C \leq 2$ mm.

(3) When changing the normalized residual indentation depth $d_{2as}/t = 1 - d_{2R}/t = 0.25–0.75$, the wedged width of the cutting part increased with d_{2as}/t, whereas the first and second stiffnesses C_1 and C_2 were almost linearly characterized with d_{2as}/t between the plain-uniform-trapezoidal blade indentation model and its half model (based on $A/C = B/C = 0.5$). This appeared to be independent of the variance of C.

(4) Bending stiffness parameters such as C_1, C_2, M_{p1} and M_{90} were characterized by the yielding stress σ_Y or its modified/updated yielding stress σ_{Y90} and the normalized residual thickness d_{2R}/t. They were strongly related to the plastic collapse moment. Herein, in the case of normal folding, the behavior of M_{90} was unpredictable from d_{2as}/t without considering the contact interference of the scored inside.

(5) The plastic-residual behavior of folding of the creasing line differed between the normal folding and reverse folding due to the difference in stress concentration and the contact interference at the scored zone. The behavior was revealed from some parameters: the angle of the first inflection point $\theta_{lp}–\theta_l$, the second stiffness C_2, the second starting angle θ_2 and the rating bending moment resistance at the right angle M_{90}.

Conflict of interest

All authors declare there is no conflict in this paper.

References

1. Hine DJ (1959) Testing boxboard creasing. *Modern Packaging* 8: 122–128.
2. Beex LAA, Peelings RHJ (2009) An experimental and computational study of creasing of paperboard. *Int J Solids Struct* 46: 4192–4207. https://doi.org/10.1016/j.ijsolstr.2009.08.012
3. Kirwan JM (2013) *Handbook of Paper and Paperboard Packaging Technology*, 2 Eds., Wiley-Blackwell, 280–292. https://doi.org/10.1002/9781118470930
4. Hashimoto T (2004) Processing technology of transparent packaging box and related problems. Carton Box 23: 44–45 (in Japanese).
5. Nagasawa S (2016) Cutting and bending of plastics sheet. *J JSTP* 57: 867–872. https://doi.org/10.9773/sosei.57.867
6. Carey KB (1992) Creasing: Turning failure into success. *Packaging Product* 1: 1–20.
7. Carlsson L, De Ruvo A, Fellers C (1983) Bending properties of creased zones of paperboard related to interlaminar defects. *J Mater Sci* 18: 1365–1373. https://doi.org/10.1007/BF01111956

8. Nagasawa S, Nasruddin M, Shiga Y (2011) Bending moment characteristics on repeated folding motion of coated paperboard scored by round-edge knife. *J Adv Mech Des Syst* 5: 385–394. https://doi.org/10.1299/jamdsm.5.385
9. Nagasawa S, Fukuzawa Y, Murayama M, et al. (2016) *Mechanics and Technology of Form Cutting for Paperboard-like Materials Processing*, Solar publishing, 101–122 (in Japanese).
10. Packaging Europe (2017) Marbach: digital zone levelling on the road to success. Available from: https://packagingeurope.com/marbach-digital-zone-levelling-on-the-road-to-success/3409.article.
11. Gahleitner M, Paulik C (2014) *Polypropylene, Ullmann's Encyclopedia of Industrial Chemistry*, Weinheim: Wiley-VCH, 1–44. https://doi.org/10.1002/14356007.o21_o04.pub2.
12. Crawford RJ (1999) *Plastics Engineering*, 3 Eds., Burlington: Elsevier Butterworth-Heinemann, 1–40.
13. Ishihara H (2010) Fundamental and application of plastics films, Converting Technical Institute, Tokyo, 33–52 (in Japanese).
14. Okuda S, Choi WS (1981) Mechanism of cutting fracture of polypropylene by impact on wedge-shaped target. *J Chem Eng Jpn* 14: 149–153. Available from: https://doi.org/10.1252/jcej.14.149.
15. Bauer W, Wüstenberg D (2002) Fracture behavior of polypropylene under dynamic cutting and shearing action in granulators. *Chem Eng Technol* 25: 1047–1051. https://doi.org/10.1002/1521-4125(20021105)25:11<1047::AID-CEAT1047>3.0.CO;2-6
16. Yamamoto A, Singprayoon S, Nagasawa S, et al. (2017) Bending behavior of polypropylene sheet subjected to two-line wedge indentation. *Trans on GIGAKU* 4: 04003/1-9. Available from: https://lib.nagaokaut.ac.jp/gigaku-press/ToG/transactions.files/TGVol4-1.pdf.
17. American Micro Industries Inc., 2021. Perforation die cutting. Available from: https://www.americanmicroinc.com/ die-cutting/perforation-die-cutting/.
18. Zimmer G (2005) Scoring/creasing plastics, *Cutting Edge* 23: 1–4. Available from: http://www.iadd.org/pages/samples/CE23-01A.htm.
19. Katayama Steel Rule Die Inc., 2022. Crease stress tester CST-J1, Available from: http://diemex.com/sale/cst.html.
20. Kudo H (1968) *Plasticity*, Morikita publishing, 16–23 (in Japanese).
21. Teng JG (1998) Plastic buckling of transition ringbeams in steel silos and tanks, In: Usami T, Itoh Y, *Stability and Ductility of Steel Structures*, Elsevier, 265–276. Available from: https://doi.org/10.1016/B978-008043320-2/50024-1.
22. Engineers Edge, 2022. Plastic Section modulus. Available from: https://www.engineersedge.com/material_science/section_modulus_12893.htm.
23. Timoshenko S (1955) Part 1: Elementary theory and problems, *Strength of Materials*, Tokyo-tosyo publishing, 144–145.
24. James MG (2001) *Mechanics of Materials*, Brooks/Cole, 615–646.